IEEE Access
Multidisciplinary | Rapid Review | Open Access Journal

Received October 10, 2018, accepted October 22, 2018, date of publication October 29, 2018,
date of current version November 30, 2018.

Digital Object Identifier 10.1109/ACCESS.2018.2878416

A Frequency Adaptive PIMR-Type Repetitive Control for a Grid-Tied Inverter

QIANGSONG ZHAO[1,2], SAINAN CHEN[1], SHENGJUN WEN[1], BOYANG QU[1], AND YONGQIANG YE[1,2], (Senior Member, IEEE)

[1]School of Electronic and Information Engineering, Zhongyuan University of Technology, Zhengzhou 450007, China
[2]College of Automation Engineering, Nanjing University of Aeronautics and Astronautics, Nanjing 211106, China

Corresponding author: Yongqiang Ye (melvinye@nuaa.edu.cn)

This work was supported in part by the National Natural Science Foundation of China under Grant 61473145, in part by the Foundation for University Key Teacher by Henan Province under Grant 2016GGJS-221, and in part by a project funded by the China Postdoctoral Science Foundation under Grant 2017M611804.

ABSTRACT A proportional integral multiresonant-type repetitive control (PIMR-type RC) has not only a better harmonic suppressing performance but also a faster error convergence rate. However, the harmonics suppressing performance of PIMR-type RC will significantly decrease when the grid fundamental frequency fluctuates in a large range. In this paper, an improved frequency adaptive PIMR-type RC (FA-PIMR-type RC) is proposed to cope with the frequency fluctuation in a large range. The improved PIMR-type RC is based on a fractional delay filter, which can be approximately realized by a finite impulse response filter. The varying fractional delay filters ensure that the resonant frequencies can match the actual reference frequency and harmonic frequencies. The synthesis, stability analysis, and parameters design criteria of the proposed FA-PIMR-type RC are given in this paper. The simulation and experimental results show that the improved PIMR-type RC can track grid reference signal, suppress harmonic signals, and have good error convergence rate under grid frequency fluctuation.

INDEX TERMS Grid-tied inverter, repetitive control (RC), FIR filter, frequency adaptive PIMR-type RC.

I. INTRODUCTION

Distributed power generation systems (DPGS), based on renewable resources, play an important role in modern power systems [1]. Grid-tied inverters in DPGS transfer a high-quality current with low total harmonic distortion (THD) into utility grid. In order to meet the requirements of current quality, various current control schemes for gird-tied inverter have been proposed, such as proportional-integral (PI) control [2], proportional resonant (PR) control [3], and repetitive control (RC) [4], [5].

PI controllers are usually used in three-phase inverters to suppress harmonics, whereas due to its limited open-loop gains at harmonic frequencies, PI controllers cannot totally reject multiple harmonics simultaneously in single-phase inverters or inverters under three-phase unbalanced conditions, which are common in DPGS.

PR controller can be utilized in both single-phase and three-phase inverters to eliminate a harmonic. However, it cannot get a good harmonic suppression performance when there are many harmonics. Multiple resonant (MR) controllers are needed to deal with several harmonics [6]–[8], but the more paralleled resonant controllers mean the smaller stability margin. Therefore, their phase compensation version is proposed [9]. Obviously, a large number of resonant controllers result in heavy computation burden and high turning complexity.

Repetitive controller, which can suppress multiple frequencies harmonics at the same time, is widely used for harmonics elimination of inverter system due to its less computational cost and design complexity, whereas the limited control gain of RC leads to a poor dynamic performance. Therefore, a PIMR-type RC scheme [10] using a modified RC plus a proportional gain is proposed. The proportional gain in PIMR-type RC scheme not only enables RC to accommodate a larger control gain and a faster error convergence rate, but also significantly improves harmonics suppressing performance.

However, the ideal PIMR-type RC is sensitive to the grid fundamental frequency fluctuation. Although the PIMR-type RC with a internal constant Q ($Q = 0.94$) can deal with grid fundamental frequency fluctuation in a small range (such as 49.8 Hz $\sim$ 50.2 Hz) [10], the THD values of grid currents will increase markedly when the grid fundamental frequency fluctuation exceeds the boundary. This is because if the deviation

between actual grid fundamental frequency and standard grid fundamental frequency (such as 50 Hz) is 0.1 Hz, the deviation of the nth harmonic frequency will be n times of 0.1 Hz, and then the control gain of the PIMR-type RC at harmonic frequencies will be finite [11]. In fact, fluctuation of the grid fundamental frequency in DPGS may exceed $\pm$ 0.2 Hz. For example, the wind DPGS should remain connected in the normal operation mode when the grid fundamental frequency is between 49 Hz $\sim$ 51 Hz for Denmark [1], which means the grid fundamental frequency may fluctuate within $\pm$ 1 Hz.

The traditional ideal repetitive controller has its digital form of $G(z) = z^{-N}/(1 - z^{-N})$, where N is the order of RC and is equal to the ratio of the sampling frequency to the fundamental frequency. However, if the sampling frequency is fixed, the order N may become a fraction when the fundamental frequency is fluctuation in practice. It is well known that repetitive controller with an integer N can only be implemented in digital control. If the nearest integer is used to approximate the fraction, there will be an error between the nearest integer and the fraction, and then the fundamental signal tracking capability and harmonics suppression capability of the traditional ideal repetitive controller will be significantly reduced.

In order to ensure the order N of RC is an integer, variable sampling frequency schemes are adopted [12]–[14]. However, the variable sampling frequency schemes will change the system dynamics and the plant model [12], and significantly increase the implementation complexity in real time.

Furthermore, some frequency-adaptive RC schemes also have been put forward to time-varying period reference to improve the robustness of RC system. In [15], an improved RC scheme with a special designed finite impulse response (FIR) filter is proposed, in which a 9th FIR filter cascaded with a traditional delay function can approximate the ideal RC function of any ratio. In [16], a high order RC is adopted to improve RC system robustness for small period variation. However, the issues are solved at the cost of adding the complexity and increasing the computational burden.

In order to improve the harmonic suppression performance of fractional-order RC with a fraction N, other frequency adaptive control schemes are developed [11], [15], [17]–[19]. In these literatures, a Lagrange-interpolation-based FIR filter [20], [21] is used to approximate the fractional-order delay item in RC. The fractional-order delay item only needs a bit of multiplications and additions for refreshing coefficient, and therefore it is fit for fast online tuning of fractional-order delay item in RC [19], [22]. However, frequency-adaptive PIMR-type RC for a grid-tied inverter has not yet been investigated.

In view of this, a frequency-adaptive PIMR-type RC (FA-PIMR-type RC) scheme based on Lagrange interpolating-polynomial-based FIR filter is proposed in this paper to improve grid-tied inverter performance. The proposed FA-PIMR-type RC scheme can simultaneously address the frequency-adaptive issue and improve error convergence rate.

II. DESCRIPTION OF AN LCL-FILTER-BASED GRID-TIED INVERTER SYSTEM

The block diagram of an LCL-filter-based grid-tied inverter system is shown in Fig. 1, where E_d is the DC bus voltage; u_{inv} is the output voltage of inverter; L_1, L_2, C are the nominal values of LCL filter, respectively; i_1 and i_2 are the currents of inductor L_1 and L_2, respectively; i_c is the capacitor current; u_g is the grid voltage; i_{ref} is reference current. A phase-locked loop (PLL) is used to provide the phase information θ of the grid voltage and the ratio N of the sampling frequency f_s to the grid frequency f_g for RC.

The parameters of the LCL-filter-based grid-tied inverter system are shown in Table. 1.

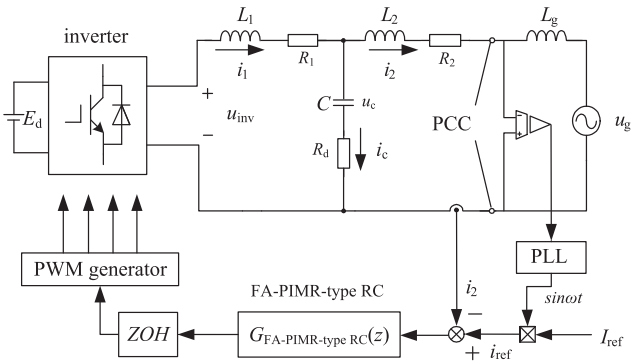

FIGURE 1. Block diagram of an LCL-filter-based grid-tied inverter with the FA-PIMR-type RC.

TABLE 1. Parameters of the LCL-filter-based grid-tied inverter.

Parameter	Value
Inverter side inductance: L_1	3 mH
L_1 equivalent resistance: R_1	0.48 Ω
Gride side inductance: L_2	2.6 mH
L_2 equivalent resistance: R_2	0.32 Ω
Filter capacitor: C	11.2 μF
DC bus voltage: E_{dc}	380 V
Grid rated frequency: f_g	50 Hz
Sampling frequency: f_s	10 kHz
Switching frequency: f_{sw}	10 kHz
Switch dead time:	3 μs

III. FRACTIONAL ORDER RC BASED ON FIR FILTER

The fractional order RC can be implemented by a fractional delay (FD) filter, where D can be separated into an integer $int(D)$ and a fraction d, as follows,

$$D = int(D) + d. \tag{1}$$

Lagrange interpolating-polynomial-based method is used to design an FIR filter for approximating a given fractional

delay z^{-d}. In this method, the delay z^{-d} is approximated by

$$z^{-d} \approx H(z) = \sum_{n=0}^{M} h(n) z^{-n}, \tag{2}$$

where M is the order of filter, $h(n)$ is the polynomial coefficient, $n = 0, 1, 2, 3, ..., M$. The implementation of Lagrange interpolating-polynomial-based FIR filter is shown in Fig. 2.

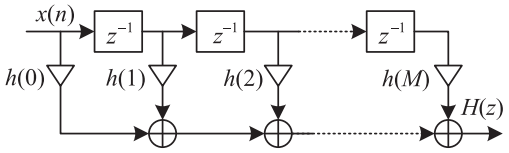

FIGURE 2. Direct form implementation of an M-order FIR filter.

As discussed by Oetken [20], filter coefficients $h(n)$ are

$$h(n) = \prod_{k=0 \bigcap k \neq n}^{M} \frac{r-k}{n-k}, n = 0, 1, 2, ..., M. \tag{3}$$

The coefficients for the Lagrange FD filters of order $M = 1$, 2, and 3 are given in the Table. 2 [21].

TABLE 2. Coefficients of the Lagrange FD filters of order $M = 1$, 2, and 3.

	M = 1	M = 2	M = 3
$h(0)$	1-d	(d-1)(d-2)/2	-(d-1)(d-2)(d-3)/6
$h(1)$	d	-d(d-2)	d(d-2)(d-3)/2
$h(2)$		d(d-1)/2	-d(d-1)(d-3)/2
$h(3)$			d(d-1)(d-2)/6

When the delay D is close to a half of the order M of FIR filter, namely $D \approx M/2$, the interpolation effect is optimal [21]. For example, if $M = 3$, $z^{-200.4}$ can be expressed as $z^{-199}z^{-1.4}$. According to Table. 2,

$$\begin{aligned} z^{-1.4} &\approx h(0)z^0 + h(1)z^{-1} + h(2)z^{-2} + h(3)z^{-3} \\ &= -0.0640 + 0.6720z^{-1} + 0.4480z^{-2} - 0.0560z^{-3}. \end{aligned} \tag{4}$$

Then, $z^{-200.4}$ is as follows,

$$\begin{aligned} z^{-200.4} &= z^{-199}z^{-1.4} \\ &= z^{-199}(-0.0640 + 0.6720z^{-1} + 0.4480z^{-2} \\ &\quad -0.0560z^{-3}). \end{aligned} \tag{5}$$

IV. FA-PIMR-TYPE RC STABILITY ANALYSIS

The PIMR-type RC [10] is composed of RC in parallel proportional gain k_p, as shown in Fig. 3. RC is used to eliminate the harmonic components and proportional gain k_p is used to improve the dynamic response and stabilize the whole control system. $Q(z)$ is an internal filter or an internal constant, z^m is the phase lead compensator that compensates the system phase lag caused by the low-pass filter and plant, k_r is the RC gain, $S(z)$ is a low-pass filter that is mainly used for high-frequency signal attenuation to enhance the RC stability. In this paper, the proposed FA-PIMR-type RC is composed of FDRC in parallel proportional gain k_p, as shown in Fig. 4. When the grid fundamental frequency is fluctuation, the proposed FA-PIMR-type RC can adjust the parameters to guarantee its the resonant frequencies to match the grid fundamental frequency and harmonic frequencies, and then have excellent signal tracking and harmonic suppression capability.

According to Fig. 4, the implementations of FA-PIMR-type RC are as follows:

① Determining the order M of the FIR filter;

② According to the grid frequency signal obtained by the PLL, the controller automatically calculates N, and then determines the value of the fractional delay d;

③ Calculating the fractional delay expressed by the integer delay according to formula (2) and Table. 2;

④ Embedding the fractional delay into the RC internal mode positive feedback to complete the frequency adaptation.

In Fig. 3, the tracking error of the PIMR-type RC system can be expressed as

$$E(z) = \frac{1}{1 + [G_{rc}(z) + k_p]P(z)}[I_{ref}(z) - U_g(z)]. \tag{6}$$

From (6), the characteristic polynomial of the system is

$$\begin{aligned} 1 + [G_{rc}(z) + k_p]P(z) &= 1 + G_{rc}(z)P(z) + k_pP(z) \\ &= [1 + k_pP(z)][1 + \frac{G_{rc}(z)P(z)}{1 + k_pP(z)}] \\ &= [1 + k_pP(z)][1 + G_{rc}(z)P_0(z)], \end{aligned} \tag{7}$$

where $P_0(z) = P(z)/[1 + k_pP(z)]$.

Thus, there are two stability conditions for the PIMR-type RC system [10]: ① the roots of polynomial $1 + k_pP(z) = 0$ are inside the unit circle; ② $|1 + G_{rc}(z)P_0(z)| \neq 0$.

The transfer function of conventional RC is

$$G_{rc}(z) = \frac{Q(z)z^{-N}}{1 - Q(z)z^{-N}} z^m k_r S(z). \tag{8}$$

According to (1), (2) and (8), the transfer function of FA-PIMR-type RC is

$$\begin{aligned} &G_{FA-PIMR-type\ RC}(z) \\ &= \frac{Q(z)z^{-D}\sum_{n=0}^{M} h(n)z^{-n}}{1 - Q(z)z^{-D}\sum_{n=0}^{M} h(n)z^{-n}} z^m k_r S(z). \end{aligned} \tag{9}$$

When $d = 0$, the FA-PIMR-type RC becomes ideal PIMR-type RC. Obviously, the stable condition ① has nothing to do with FA-PIMR-type RC. Substitute (8) into condition ②

$$|1 - Q(z)z^{-N} + k_rQ(z)z^{-N+m}S(z)P_0(z)| \neq 0. \tag{10}$$

Then, (10) can be rewritten as

$$\begin{aligned} &|Q(z)z^{-N}(1 - z^m k_r S(z)P_0(z))| < 1, \\ &\forall z = e^{j\omega T}, 0 < \omega < \frac{\pi}{T}. \end{aligned} \tag{11}$$

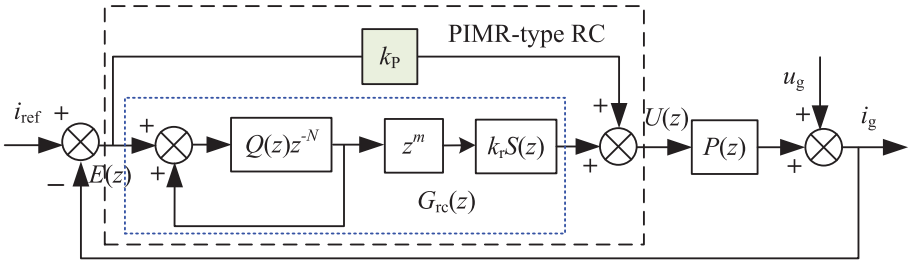

FIGURE 3. Block diagram of the PIMR-tpye RC scheme.

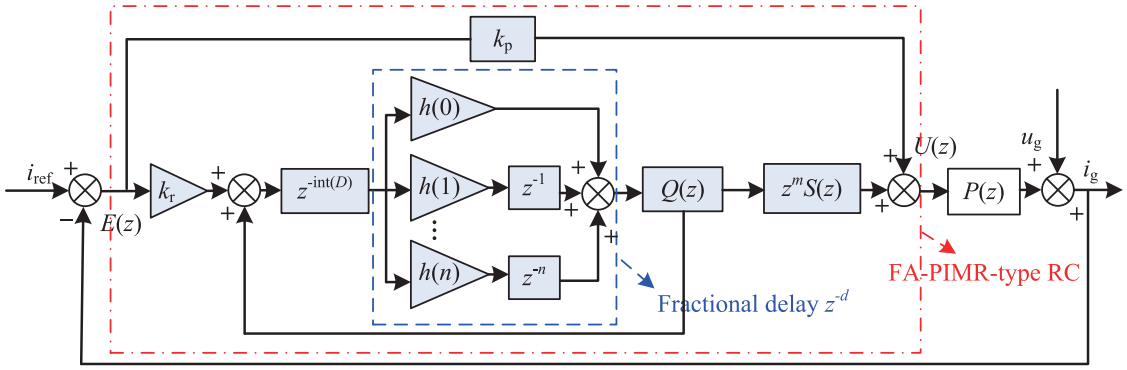

FIGURE 4. Block diagram of the FA-PIMR-tpye RC scheme.

TABLE 3. The corresponding RC delay *N* when the grid frequency changes.

Frequency (Hz)	49.5	49.6	49.7	49.8	49.9	50	50.1	50.2	50.3	50.4	50.5
N	202	201.6	201.2	200.8	200.4	200	199.6	199.2	198.8	198.4	198

If the frequency of reference signal $i_{ref}(t)$ and disturbance $u_g(t)$ approaches $\omega_l = 2\pi l/N$, with $l = 0, 1, 2, \ldots, L$ ($L = N/2$ for even N and $L = (N-1)/2$ for odd N), then $z^N = 1$ [23]. Consequently, we have

$$|Q(z)(1 - z^m k_r S(z) P_0(z))| < 1, \quad \forall z = e^{j\omega T}. \tag{12}$$

Substitute (2) into (11), we obtain

$$|Q(z)z^{-D}\sum_{n=0}^{M} h(n)z^{-n}(1 - k_r z^m S(z)P_0(z))| < 1, \quad \forall z = e^{j\omega T}, 0 < \omega < \frac{\pi}{T}. \tag{13}$$

Then, (13) can be rewritten as

$$|Q(z)(1 - z^m k_r S(z)P_0(z))| < |z^{-D}\sum_{n=0}^{M} h(n)z^{-n}|^{-1}. \tag{14}$$

It can be seen from (2) that within the FD filter bandwidth, $|z^{-D}\sum_{n=0}^{M} h(n)z^{-n}|^{-1} \to 1$. The stable condition of the FA-PIMR-type RC system is the same as that of the PIMR-type RC system.

When the sampling frequency is 10 kHz and the grid frequency is varying between 49.5 Hz and 50.5 Hz, the values of N is shown in Table. 3. It can be seen that N will fluctuate between 202 and 198 when the grid frequency changes, and N will be fractions except three frequencies, i.e. 49.5 Hz, 50 Hz, and 50.5 Hz. If the nearest integer is used to approximate the fraction, there will be an error between the nearest integer and the fraction. Therefore, it is necessary to implement the fractional delay to further reduce the error.

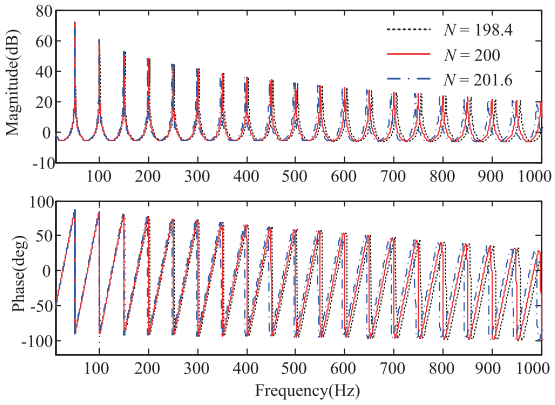

FIGURE 5. Bode diagrams of PIMR-type RC ($N = 200$) and FA-PIMR-type RC ($N = 198.4$ and 201.6).

The frequency characteristics of the ideal PIMR-type RC ($N = 200$) and FA-PIMR-type RC ($N = 198.4$ and $N = 201.6$)

are shown in Fig. 5, respectively. Fig. 5 shows that the deviation between the ideal PIMR-type RC and the FA-PIMR-type RC at a certain frequency is increasing along with the increase of frequency, which means there will be a big deviation at high frequency if there is a little deviation at fundamental frequency. Therefore, the harmonic suppressing performance of ideal PIMR-type RC will deteriorate at high frequency when the fundamental frequency fluctuates.

The frequency characteristics of ideal PIMR-type RC and FA-PIMR-type RC in the neighborhood of 9th harmonic frequency are shown in Fig. 6. It shows that when the fundamental frequency is 50 Hz, the open-loop gain of ideal PIMR-type RC at 9th harmonic frequency is 35 dB. However, when the fundamental frequency fluctuates from 50 Hz to 50 $\pm$ 0.4 Hz, the open-loop gain of the ideal PIMR-type RC at 9th harmonic frequency (446.4 Hz or 453.6 Hz) will drop down to 8 dB, whereas that of the FA-PIMR-type RC can remain 35 dB at 9th harmonic frequency. Obviously, the FA-PIMR-type RC will have a better harmonics suppressing performance than the ideal PIMR-type RC.

V. SIMULATION

In order to compare the performance of FA-PIMR-type RC with PIMR-type RC when the grid frequency fluctuates, two control methods are verified in the MATLAB/Simulink. The PIMR-type RC system model is shown in Fig. 3. The parameters of the inverter system are shown in Table. 1. The controller parameters are as follows: the parallel proportional gain k_p = 19, the RC gain k_r = 16, the internal mode $Q(z) = (z + 2 + z^{-1})/4$ which is different from $Q(z) = 0.94$ in [10], the phase lead compensation m = 9, the compensator $S(z)$ is a fourth-order Butterworth low-pass filter (cutoff frequency 1 kHz). The sampling frequency f_s = 10 kHz, the rated frequency of the power grid f_g = 50 Hz. The magnitude of the reference current is 10 A.

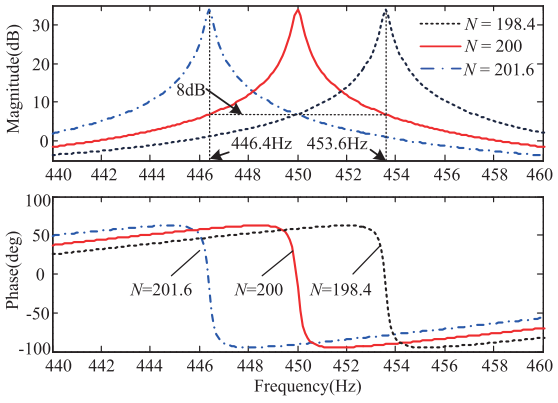

FIGURE 6. Frequency characteristics of PIMR-type RC (N = 200) and FA-PIMR-type RC (N = 198.4 and 201.6) at 9th harmonic frequency.

A. THE GRID FREQUENCY IS 49.6 HZ

When the grid frequency is 49.6 Hz, N is 201.6. The reference current and output current are shown in Fig. 7. The PIMR-type RC is the same as FA-PIMR-type RC can track the reference current in 0.06 s. The reference current from 0.4 s to 0.44 s are shown in Fig. 8, the output current of FA-PIMR-type RC has some distortion due to harmonics, whereas it is better than that of the PIMR-type RC system. The spectrum analysis of the output current is shown in Fig. 9. The THD of the PIMR-type RC is 3.68%, which satisfies the standard of 5% in the IEEE Std 1547, whereas the low frequency harmonics is very high. The THD of the FA-PIMR-type RC output current is 1.57%, and the percent of single odd harmonic below is less than 0.2%, which is much lower than that in the PIMR-type RC system. The current error convergence is shown in Fig. 10. Obviously, the current tracking error of the PIMR-type RC system in Fig. 10 is 1.2 A, which is bigger than that of the FA-PIMR-type RC system in Fig. 10. Therefore, the FA-PIMR-type RC system greatly improves the output current.

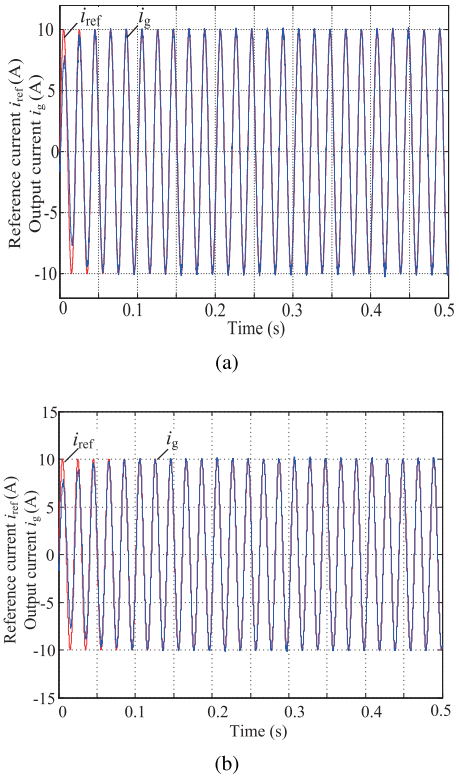

FIGURE 7. Reference current and output current with different control schemes: (a). PIMR-type RC; (b). FA-PIMR-type RC.

B. THE GRID FREQUENCY IS 50.4 HZ

When the grid frequency is 50.4 Hz, N is 198.4. As shown in Fig. 11, the output current of FA-PIMR-type RC can track the reference current in 0.06 s. As shown in Fig. 12, the output current of the FA-PIMR-type RC system is clearly superior to the PIMR-type RC system. As shown in Fig. 13, the output current of the PIMR-type RC system still contains some low frequency odd harmonic, and the THD is 4.17%, whereas the FA-PIMR-type RC system are significantly reduced, which are less than 0.3%, and the THD is only 1.34%. As shown

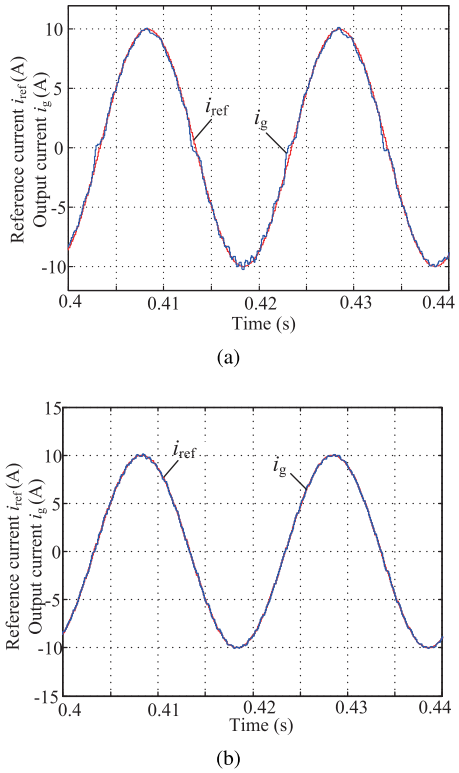

FIGURE 8. Reference current and output current with different control schemes (0.4 s - 0.44 s): (a). PIMR-type RC; (b). FA-PIMR-type RC.

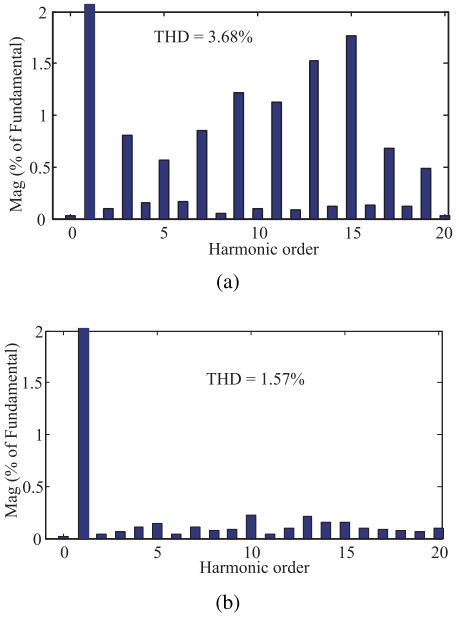

FIGURE 9. Spectrum analysis of output current with different control systems: (a). PIMR-type RC; (b). FA-PIMR-type RC.

in Fig. 14, both schemes have the same dynamic response speed. However, the steady-state error of the FA-PIMR-type RC system is 0.4 A, while that of the PIMR-type RC system is 0.8 A. Obviously, the FA-PIMR-type RC system has smaller steady-state error.

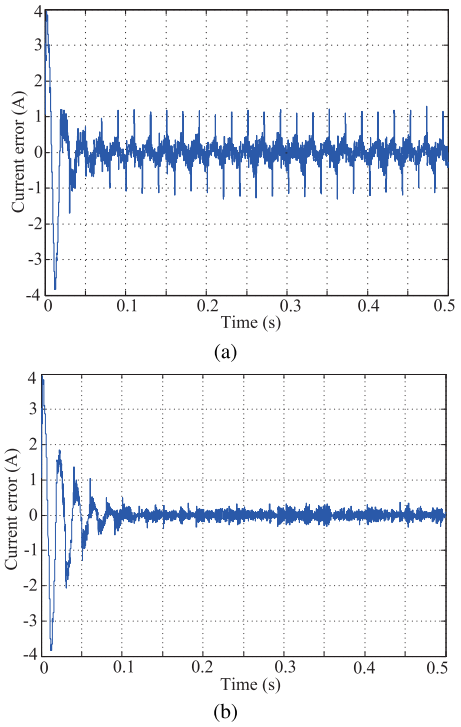

FIGURE 10. Current error convergence with different control systems: (a). PIMR-type RC; (b). FA-PIMR-type RC.

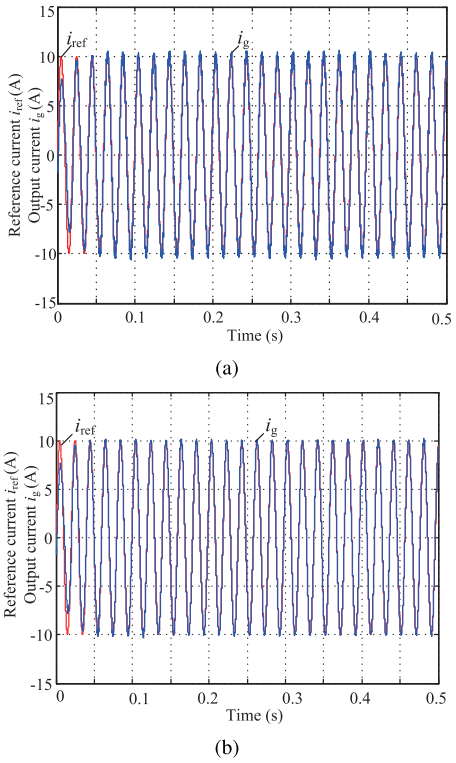

FIGURE 11. Reference current and output current with different control schemes: (a). PIMR-type RC; (b). FA-PIMR-type RC.

VI. EXPERIMENTAL RESULTS

In order to further verify the theoretical analysis and simulation results, the experimental setup is shown in Fig. 15.

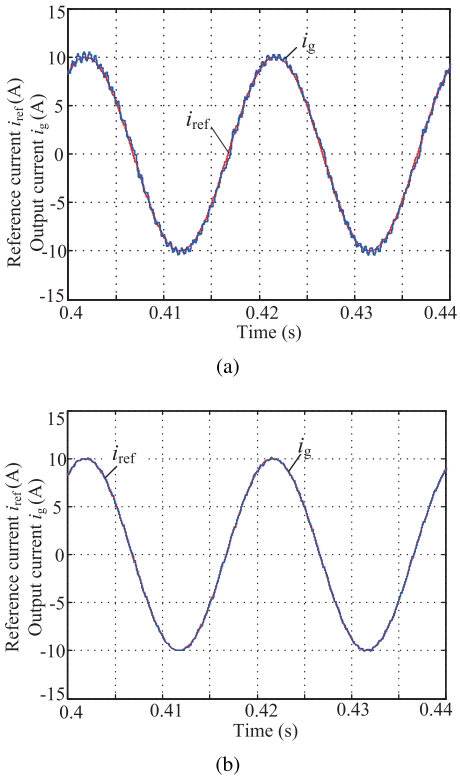

FIGURE 12. Reference current and output current with different control schemes (0.4 s - 0.44 s): (a). PIMR-type RC; (b). FA-PIMR-type RC.

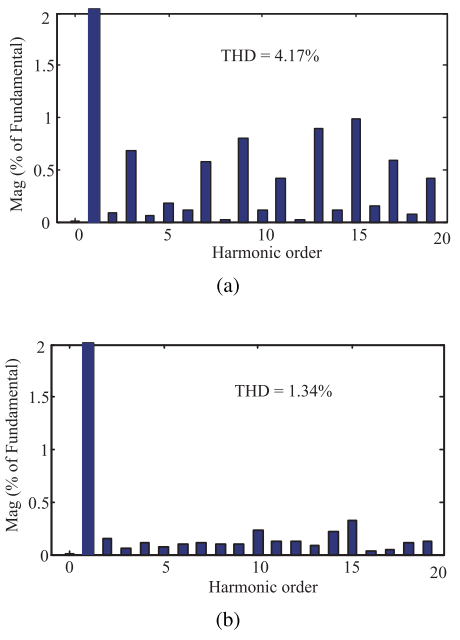

FIGURE 13. Spectrum analysis of output current with different control systems: (a). PIMR-type RC; (b). FA-PIMR-type RC.

The experimental setup comprises an IGBT inverter bridge, an LCL filter, voltage and current sensors, a DATA Acquisition board (DAQ Quanser QPIDe), and a PC with QuaRC and MATLAB/Simulink. It is difficult to change the grid fundamental frequency artificially in practice. According to [15], the sampling frequency is changed to simulate the grid frequency variation in this paper. The performances of the PIMR-type RC and the FA-PIMR-type RC are verified when N is 198.4 and N is 201.6, respectively.

A. N = 198.4

When N is 198.4, the output current of the PIMR-type RC system and its spectrum are shown in Fig. 16.

As can be seen from Fig. 16, due to the dead time of switching device and the background harmonics of grid, the THD of the output current of PIMR-type RC system is 4.93%, which is close to the upper limit of the grid-tied current standard of 5%. It can be seen the odd harmonic content of low frequency is high, especially the 11th harmonic content reaches 2.5%, which has exceeded the upper limit of 2.0% in IEEE Std-1547. Because the harmonic suppressing performance of the PIMR-type RC decreases when the fundamental frequency fluctuates in a large range, low frequency harmonic content of the output current is high. The output current of the FA-PIMR-type RC system and its spectrum are shown in Fig. 17, the output current THD is 2.15%, and the single harmonic content below 19th is less than 0.6%, and the waveform is significantly better than the PIMR-type RC system.

B. N = 201.6

When N is 201.6, the output current of the PIMR-type RC system and its spectrum are shown in Fig. 18. The output

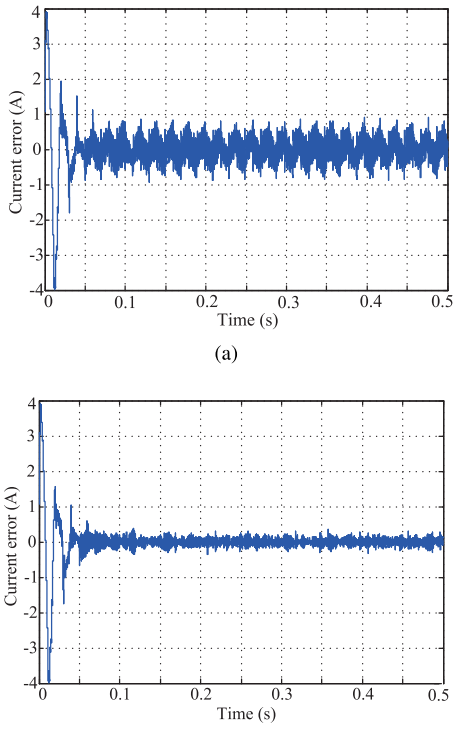

FIGURE 14. Current error convergence with different control systems: (a). PIMR-type RC; (b). FA-PIMR-type RC.

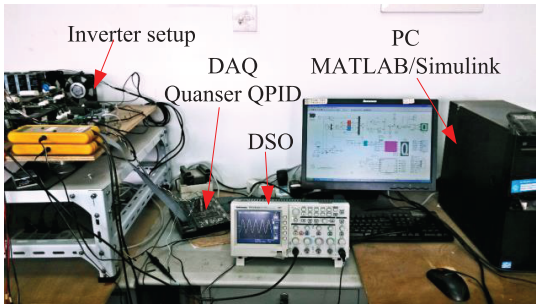

FIGURE 15. Experimental setup.

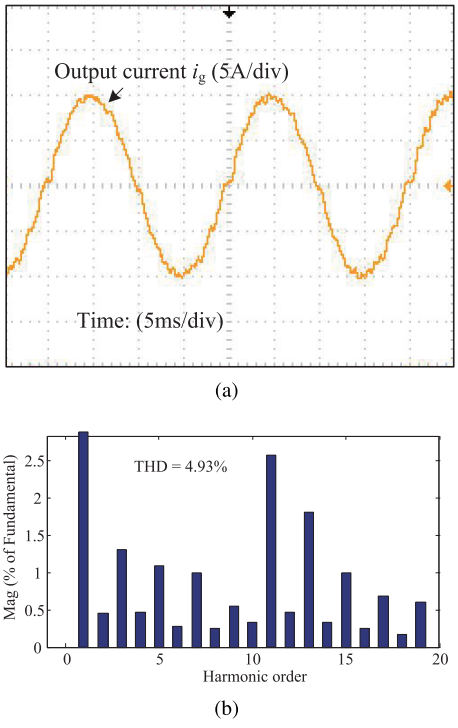

FIGURE 16. Output current and its spectrum of PIMR-type RC system when $N = 198.4$.

current of the FA-PIMR-type RC system and its spectrum are shown in Fig. 19.

As can be seen from Fig. 18, the THD of the output current of the PIMR-type RC system is 5.78% when N is 201.6, and the single harmonic content of 11th, 13th, and 15th are more than 2.0%, which exceed the THD standard in IEEE Std-1547. The THD of the output current of the FA-PIMR-type RC system is 1.99% which is lower than that of the PIMR-type RC system. Also the single harmonic content below 19th is less than 0.5%, which is far lower than IEEE Std-1547. This is because the FA-PIMR-type RC system can provide high-gain at the grid fundamental frequency and its harmonics frequencies, so it has excellent signal tracking capability and harmonics suppression capability.

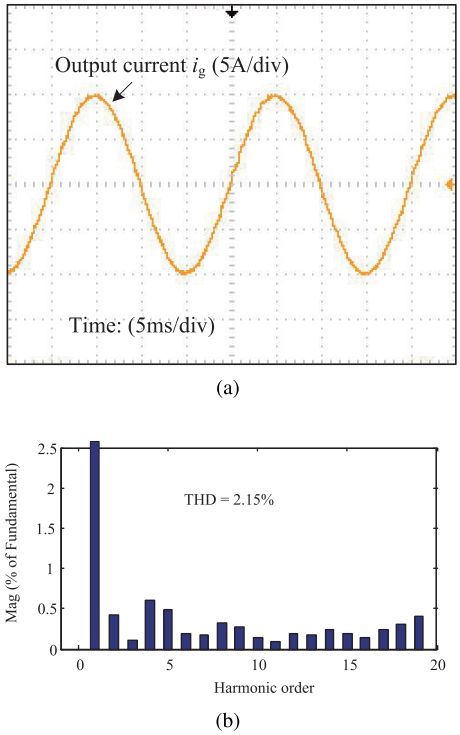

FIGURE 17. Output current and its spectrum of FA-PIMR-type RC system when $N = 198.4$.

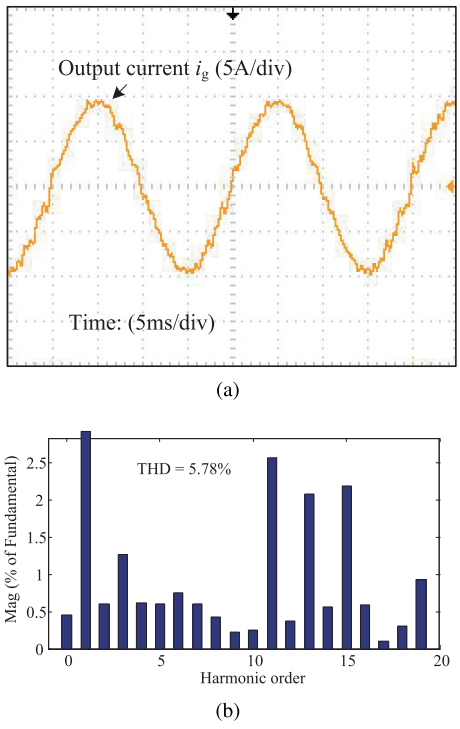

FIGURE 18. Output current and its spectrum of PIMR-type RC system when $N = 201.6$.

VII. FA-PIMR-TYPE RC APPLICATION

When the grid frequency f_g is varied from 49.5 Hz to 50.5 Hz and the sampling frequency f_s is 10 kHz, the N varies from

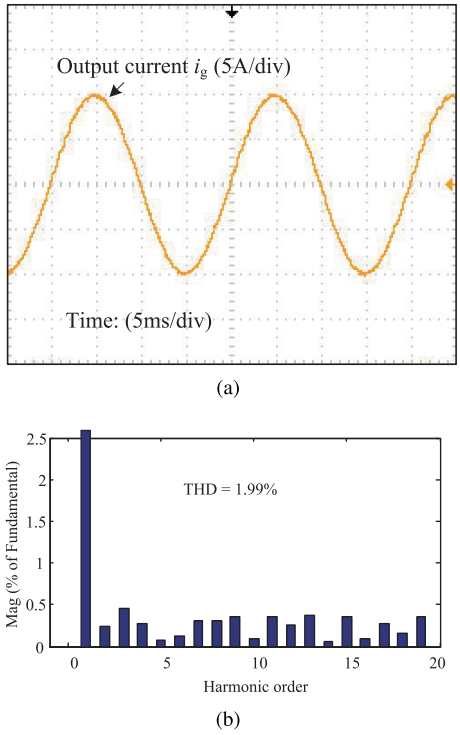

FIGURE 19. Output current and its spectrum of FA-PIMR-type RC system when $N = 201.6$.

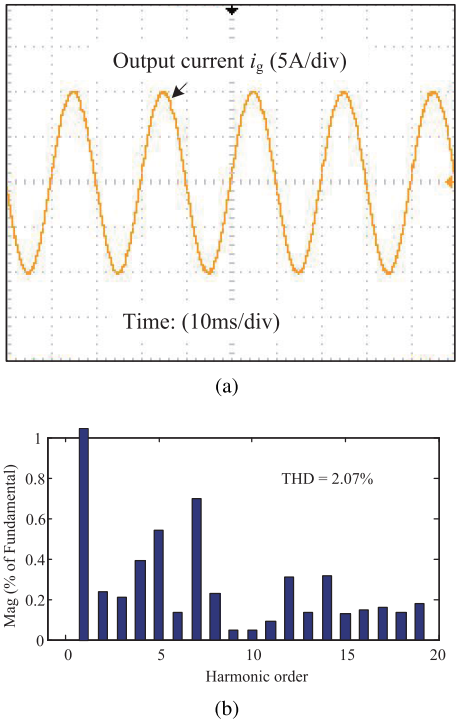

FIGURE 20. Output current and its spectrum of FA-PIMR-type RC system when $N = 201.2$.

202 to 198. In order to verify the effect of the FA-PIMR-type RC, changing the sampling frequency f_s of the control system is adopted to simulate the variation of N in a certain range. When f_g is fixed, the sampling frequency f_s varying from 10100 to 9900.

When the sampling frequency f_s is 10060, corresponding to N is 201.2, the output current of FA-PIMR-type RC system and its spectrum are shown in Fig. 20.

According to Fig. 20, the FA-PIMR-type RC system can track the reference current when the delay is 201.2. The THD of the output current is 2.07%, and the values of 5th and 7th harmonics are higher than 0.5%, but it does not exceed the standard of 4.0% (below 11th) in IEEE Std-1547.

When the sampling frequency f_s is 9940, the corresponding N is 198.8, the output current of FA-PIMR-type RC system and its spectrum are shown in Fig. 21.

According to Fig. 21, the FA-PIMR-type RC system can track the reference current when the delay is 198.8. The THD of the output current is 2.45%, and the values of 5th and 7th harmonics are about 0.5% and 0.9%, respectively, but far below the standard of 4.0% (below 11th) in IEEE Std-1547.

It can be concluded from Fig. 20 and Fig. 21 that the number N of RC is a fraction when the grid frequency changes within a certain range, the FA-PIMR-type RC system has a good reference current tracking capability and an excellent harmonics suppression capability.

In order to verify the dynamics of the proposed FA-PIMR-type RC, when the reference current amplitude drops from

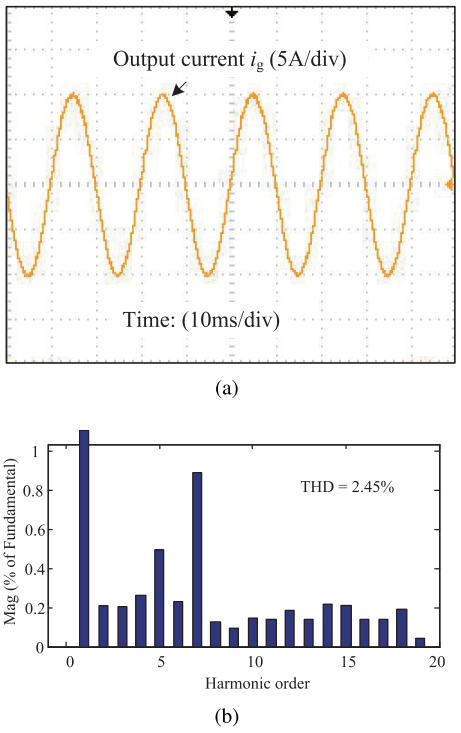

FIGURE 21. Output current and its spectrum of FA-PIMR-type RC system when $N = 198.8$.

10 A to 6 A, the output current is shown in Fig. 22, and the output current tends to be stable after 2 to 3 fundamental frequency periods (about 50 ms).

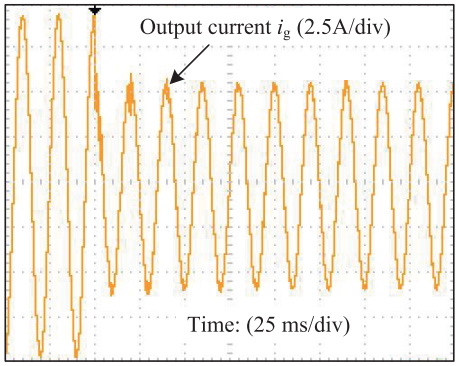

FIGURE 22. Output current of FA-PIMR-type RC system when reference current amplitude changes.

VIII. CONCLUSION

In this paper, a frequency adaptive PIMR-type RC for a grid-tied inverter is proposed. The FA-PIMR-type RC is based on fractional delay filter which can be approximately realized by FIR filter. The stability of the FA-PIMR-type RC is analyzed and the implementation of new controller is given. The simulation and experimental results show that the proposed FA-PIMR-type RC can provide a higher gain at fundamental grid frequency and harmonics frequencies than the PIMR-type RC when grid frequency fluctuates, and then have a good reference current tracking capability and an excellent harmonics suppression capability.

REFERENCES

[1] F. Blaabjerg, Y. Yang, D. Yang, and X. Wang, "Distributed power-generation systems and protection," *Proc. IEEE*, vol. 105, no. 7, pp. 1311–1331, Jul. 2017.

[2] J. Dannehl, C. Wessels, and F. W. Fuchs, "Limitations of voltage-oriented PI current control of grid-connected PWM rectifiers with LCL filters," *IEEE Trans. Ind. Electron.*, vol. 56, no. 2, pp. 380–388, Feb. 2009.

[3] L. Herman, I. Papic, and B. Blazic, "A proportional-resonant current controller for selective harmonic compensation in a hybrid active power filter," *IEEE Trans. Power Del.*, vol. 29, no. 5, pp. 2055–2065, Oct. 2014.

[4] G. Escobar, M. Hernandez-Gomez, A. A. Valdez-Fernandez, M. J. Lopez-Sanchez, and G. A. Catzin-Contreras, "Implementation of a $6n \pm 1$ repetitive controller subject to fractional delays," *IEEE Trans. Ind. Electron.*, vol. 62, no. 1, pp. 444–452, Jan. 2015.

[5] P. M. de Almeida, J. L. Duarte, P. F. Ribeiro, and P. G. Barbosa, "Repetitive controller for improving grid-connected photovoltaic systems," *IET Power Electron.*, vol. 7, no. 6, pp. 1466–1474, Jun. 2014.

[6] A. G. Yepes, F. D. Freijedo, O. Lopez, and J. Doval-Gandoy, "High-performance digital resonant controllers implemented with two integrators," *IEEE Trans. Power Electron.*, vol. 26, no. 2, pp. 563–576, Feb. 2011.

[7] S. Li, X. Wang, Z. Yao, T. Li, and Z. Peng, "Circulating current suppressing strategy for MMC-HVDC based on nonideal proportional resonant controllers under unbalanced grid conditions," *IEEE Trans. Power Electron.*, vol. 30, no. 1, pp. 387–397, Jan. 2015.

[8] L. F. A. Pereira, J. V. Flores, G. Bonan, D. F. Coutinho, and J. M. G. da Silva, "Multiple resonant controllers for uninterruptible power supplies—A systematic robust control design approach," *IEEE Trans. Ind. Electron.*, vol. 61, no. 3, pp. 1528–1538, Mar. 2014.

[9] Y. H. Yang, K. Zhou, M. Cheng, and B. Zhang, "Phase compensation multiresonant control of CVCF PWM converters," *IEEE Trans. Power Electron.*, vol. 28, no. 8, pp. 3923–3930, Aug. 2013.

[10] Q. Zhao and Y. Ye, "A PIMR-type repetitive control for a grid-tied inverter: Structure, analysis, and design," *IEEE Trans. Power Electron.*, vol. 33, no. 3, pp. 2730–2739, Mar. 2018.

[11] Y. Yang, K. Zhou, and F. Blaabjerg, "Enhancing the frequency adaptability of periodic current controllers with a fixed sampling rate for grid-connected power converters," *IEEE Trans. Power Electron.*, vol. 31, no. 10, pp. 7273–7285, Oct. 2016.

[12] J. Olm, G. Ramos, and R. Costa-Castello, "Stability analysis of digital repetitive control systems under time-varying sampling period," *IET Control Theory Appl.*, vol. 5, no. 1, pp. 29–37, 2011.

[13] E. Kurniawan, Z. Cao, and Z. Man, "Design of robust repetitive control with time-varying sampling periods," *IEEE Trans. Ind. Electron.*, vol. 61, no. 6, pp. 2834–2841, Jun. 2014.

[14] T. Hornik and Q. Zhong, "A current-control strategy for voltage-source inverters in microgrids based on $H^{\infty}$and repetitive control," *IEEE Trans. Power Electron.*, vol. 26, no. 3, pp. 943–952, Mar. 2011.

[15] D. Chen, J. Zhang, and Z. Qian, "An improved repetitive control scheme for grid-connected inverter with frequency-adaptive capability," *IEEE Trans. Ind. Electron.*, vol. 60, no. 2, pp. 814–823, Feb. 2013.

[16] M. Steinbuch, S. Weiland, and T. Singh, "Design of noise and period-time robust high-order repetitive control, with application to optical storage," *Automatica*, vol. 43, no. 12, pp. 2086–2095, 2007.

[17] M. Abusara, S. Sharkh, and P. Zanchetta, "Adaptive repetitive control with feedforward scheme for grid-connected inverters," *IET Power Electron.*, vol. 8, no. 8, pp. 1403–1410, 2015.

[18] Q. Zhao, Y. Ye, G. Xu, and M. Zhu, "Improved repetitive control scheme for grid-connected inverter with frequency adaptation," *IET Power Electron.*, vol. 9, no. 5, pp. 883–890, Apr. 2016.

[19] Z. X. Zou, K. Zhou, Z. Wang, and M. Cheng, "Frequency-adaptive fractional-order repetitive control of shunt active power filters," *IEEE Trans. Ind. Electron.*, vol. 62, no. 3, pp. 1659–1668, Mar. 2015.

[20] G. Oetken, "A new approach for the design of digital interpolating filters," *IEEE Trans. Acoust., Speech, Signal Process.*, vol. ASSP-27, no. 6, pp. 637–643, Dec. 1979.

[21] T. I. Laakso, V. Valimaki, M. Karjalainen, and U. K. Laine, "Splitting the unit delay [FIR/all pass filters design]," *IEEE Signal Process. Mag.*, vol. 13, no. 1, pp. 30–60, Jan. 1996.

[22] C. Xie, X. Zhao, M. Savaghebi, L. Meng, J. M. Guerrero, and J. C. Vasquez, "Multirate fractional-order repetitive control of shunt active power filter suitable for microgrid applications," *IEEE J. Emerg. Sel. Topics Power Electronics*, vol. 5, no. 2, pp. 809–819, Jun. 2017.

[23] B. Zhang, D. Wang, K. Zhou, and Y. Wang, "Linear phase lead compensation repetitive control of a CVCF PWM inverter," *IEEE Trans. Ind. Electron.*, vol. 55, no. 4, pp. 1595–1602, Apr. 2008.

QIANGSONG ZHAO was born in Kaifeng, China. He received the B.E. and M.E. degrees in electrical engineering from the Zhongyuan University of Technology, Zhengzhou, China, in 2006 and 2009, respectively, and the Ph.D. degree in control theory and control engineering from the Nanjing University of Aeronautics and Astronautics, Nanjing, China, in 2016.

Since 2016, he has been an Associate Professor with the School of Electronic and Information, Zhongyuan University of Technology. Since 2017, he has also been a Post-Doctoral Research Fellow with the College of Automation Engineering, Nanjing University of Aeronautics and Astronautics. His research interests include power converters for renewable energy applications, control of power electronic converters, and advanced control and its applications.

SAINAN CHEN was born in Pingdingshan, China. She received the B.E. degree in automation from the College of Information and Business, Zhongyuan University of Technology, Zhengzhou, China, in 2016, where she is currently pursuing the master's degree in control engineering. Her research interests include power converters for renewable energy applications and control of power electronic converters.

SHENGJUN WEN received the Ph.D. degree in electronic and information engineering from the Graduate School of Engineering, Tokyo University of Agriculture and Technology and Okayama University, in 2011. He is currently an Associate professor with the Zhongyuan-Petersburg Aviation College, Zhongyuan University of Technology. He has taken part in five research projects since 2011, for example research project on support vector machine and safety control technology. And more than 60 academic papers have been published. Until now, he was in charge of some courses for graduate and undergraduate students, such as computer control, industrial computer and networked control, and intelligent control. His research interests include nonlinear control, safety control, and networked control. In 2011, he received a research scholarship sponsored by the WESCO Scientific Promotion Foundation and a National Scholarship for Privately Financed International Students Sponsored by the Ministry of Education, Culture, Sports, Science and Technology.

BOYANG QU received the B.E. and Ph.D. degrees from the School of Electrical and Electronic Engineering, Nanyang Technological University, Singapore. He is currently an Associate Professor with the School of Electric and Information Engineering, Zhongyuan University of Technology, China. His research interests include machine learning, neural network, genetic and evolutionary algorithms, swarm intelligence, multi-objective optimization, and signal processing.

YONGQIANG YE (M'06–SM'12) was born in Tongxiang, China. He received the B.E. and M.Sc.Eng. degrees from Zhejiang University, Hangzhou, China, in 1994 and 1997, respectively, and the Ph.D. degree from Nanyang Technological University, Singapore, in 2004, all in electrical engineering.

He was a Faculty Member with the School of Information, Zhejiang University of Finance and Economics, Hangzhou, China, for more than four years. He had also been a Post-Doctoral Research Fellow with the Department of Electrical Engineering, Lakehead University, Thunder Bay, ON, Canada, the Department of Systems and Computer Engineering, Carleton University, Ottawa, ON, Canada, and the Department of Mechanical Engineering, Dalhousie University, Halifax, NS, Canada. Since 2009, he has been a Professor with the College of Automation Engineering, Nanjing University of Aeronautics and Astronautics, Nanjing, China. He is currently a Distinguished Professor of Henan Province affiliated with the School of Electronic and Information, Zhongyuan University of Technology, Zhengzhou, China. He has authored or co-authored one book and more than 70 journal papers. His current research interests include advanced control of power electronics and electrical machines.